(Preprint) AAS 22-759

ADVANCES IN KOOPMAN OPERATOR THEORY FOR OPTIMAL CONTROL PROBLEMS IN SPACE FLIGHT

Christian Hofmann[*], Simone Servadio[†], Richard Linares[‡], and Francesco Topputo[§]

A framework is presented where a nonlinear dynamical system is transformed into a higher-dimensional bilinear system using the Koopman operator theory. The nonlinear dynamics are projected onto a set of orthogonal polynomials via the Galerkin method to obtain the evolution of the eigenfunctions, so that the time evolution of any observable is described as a linear combination of the basis functions. The method is applied to the low-thrust trajectory optimization problem using a new set of orbital elements. The accuracy of the transformed system is analyzed, and an example transfer to an asteroid is solved to assess the performance.

INTRODUCTION

In the past decades, not only the number, but also the complexity of space missions has grown tremendously. The development of new electric propulsion systems that provide only low thrust has lead to various new space missions such as NASA's Deep Space 1 [1] and DART [2], or ESA's SMART 1 missions [3]. Especially CubeSats have become increasingly important due to their low cost; a multitude of new missions is foreseen in the near future [4, 5]. Despite their severe limitations, CubeSats are now a viable alternative for many space missions [6]. The main advantage of low-thrust propulsion is the high specific impulse that can provide a large total Δv, enabling new missions that would not be feasible with conventional chemical propulsion. As the state of the spacecraft changes only slowly due to the small control actions, transfer times increase because the thruster has to operate over a significantly larger portion of the flight time. This causes new challenges and requires new trajectory design techniques.

Designing a low-thrust trajectory is a complex task as it requires solving a nonlinear optimal control problem. At the same time, obtaining solutions quickly and reliably is required in many applications [7–10]. Direct and indirect methods are most commonly used to solve the low-thrust trajectory optimization problem [11]. The optimal control problem is transformed into a parameter optimization or two-point boundary value problem and solved numerically using some gradient-based technique. Due to the highly nonlinear dynamics and often complex constraints, finding an

[*]Ph.D. Candidate, Department of Aerospace Science and Technology, Politecnico di Milano, 20156 Milan, Italy. Email: christian.hofmann@polimi.it

[†]Postdoctoral Associate, Department of Aeronautics and Astronautics, Massachusetts Institute of Technology, Cambridge, MA 02139, USA. Email: simoserv@mit.edu

[‡]Associate Professor, Department of Aeronautics and Astronautics, Massachusetts Institute of Technology, Cambridge, MA 02139, USA. Email: linaresr@mit.edu

[§]Professor, Department of Aerospace Science and Technology, Politecnico di Milano, 20156 Milan, Italy. Email: francesco.topputo@polimi.it

optimal solution is still a challenging task as both approaches require a decent initial guess. For this reason, approximate solutions using simplified models (e.g., Kepler or Stark model [12]), predefined state or control profiles (e.g., shape-based methods [13] or constant radial and tangential thrust [14]) are often sought to generate the initial guess. However, these problems are still highly nonlinear and difficult to solve.

In the past decade, convex programming has become a promising technique as it combines high robustness, good accuracy, and low computational effort [15, 16]. Still, this approach requires all constraints to be convex. Even though many constraints can be relaxed and convexified, handling nonlinear dynamics properly is still a challenge [17]. As a consequence, dynamics are usually approximated using a first-order Taylor series [18]. This, however, is only a local approximation and can result in non-convergence if a poor initial guess is provided. How to deal with nonlinear and non-convex dynamics in engineering problems is therefore a major challenge.

For this reason, linearization techniques have attracted a lot of attention in the last few years [19, 20]. Especially lifting nonlinear systems into a higher-dimensional space has become increasingly important as this allows us to represent a nonlinear system as a linear one, and sophisticated linear system theory can be applied. One drawback, however, is the higher (often infinite) dimensional space of the transformed system. An important lifting technique is the linear, infinite-dimensional Koopman operator that describes the evolution of observable functions [21]. It has been applied to various problems in engineering, e.g. estimation [22], robotics [23], and fluid dynamics [24]. Despite the increasing popularity, its application in astrodynamics is very limited due to the high accuracy required; standard data-driven approaches cannot achieve this [25]. Recently, the zonal harmonics problem has been solved using Koopman operator theory (KOT) [26]. In addition, it has been applied to attitude dynamics [27] and the motion of satellites around libration points [28]. However, KOT has mainly been used for the prediction and estimation of nonlinear systems without considering an external control. Therefore, this work investigates how the benefits of KOT can be used in modern optimal control theory, and how the current challenges can be overcome. A recently developed set of orbital elements is modified and extended to allow for perturbing accelerations. The theory of KOT is explained and then applied to the low-thrust trajectory optimization problem. A direct method is used to solve the corresponding optimal control problem. We compute planar interplanetary transfers to demonstrate the effectiveness of the approach. Even though the low-thrust trajectory optimization problem is considered as an application, the theory presented in this paper may be applied to other applications in space flight, such as powered descent guidance problems.

The paper is structured as follows. Section II describes the general Koopman operator theory. In Section III, the set of orbital elements is explained and the low-thrust trajectory optimization problem is stated. Section IV addresses how KOT is applied to the optimal control problem, and Section V presents the results of the numerical simulations. Section VI concludes this paper.

KOOPMAN OPERATOR THEORY

The Koopman operator is an infinite-dimensional, linear operator that describes the evolution of observable functions. Given a general nonlinear dynamical system

$$\frac{\mathrm{d}\mathbf{x}(t)}{\mathrm{d}t} = \mathbf{f}(\mathbf{x}), \quad \mathbf{x}(t_0) = \mathbf{x}_0 \tag{1}$$

where $\mathbf{x} \in \mathbb{R}^n$ and $\mathbf{f} \in \mathbb{R}^n$ are defined in the n-dimensional state space. Let $g(\mathbf{x})$ be an observable function. KOT describes how these functions evolve in an extended, infinite-dimensional Hilbert

space [20]:

$$\frac{\mathrm{d}g(\mathbf{x})}{\mathrm{d}t} = \mathcal{K}(g(\mathbf{x})) = (\nabla_{\mathbf{x}} g(\mathbf{x}))\frac{\mathrm{d}\mathbf{x}(t)}{\mathrm{d}t} = (\nabla_{\mathbf{x}} g(\mathbf{x}))\mathbf{f}(\mathbf{x}) \tag{2}$$

where $\mathcal{K}$ is the Koopman operator. The following relationship holds as the operator is linear:

$$\mathcal{K}\left(c_1 g_1(\mathbf{x}) + c_2 g_2(\mathbf{x})\right) = c_1\mathcal{K}(g_1(\mathbf{x})) + c_2\mathcal{K}(g_2(\mathbf{x})) \tag{3}$$

with constants c_1 and c_2. The major goal is to find a new set of coordinates that result in a linear representation of the dynamics. Due to the linear property, it is possible to perform an eigendecomposition:

$$\mathcal{K}\phi = \frac{\mathrm{d}\phi(\mathbf{x})}{\mathrm{d}t} = (\nabla_{\mathbf{x}}\phi(\mathbf{x}))\frac{\mathrm{d}\mathbf{x}(t)}{\mathrm{d}t} = \lambda\phi(\mathbf{x}) \tag{4}$$

where ϕ are the right eigenfunctions. The evolution of the system is therefore given by combinations of the eigenfunctions. If each component of the vector valued function $\mathbf{g}$ lies in the span of the eigenfunctions, it can be written as

$$\mathbf{g}(\mathbf{x}) = \sum_{i=1}^{\infty} \phi_i(\mathbf{x})\mathbf{v}_j \tag{5}$$

Once the eigenfunctions are known, the evolution of the observables is given by Eq. (4) where the observables are projected onto the span of the eigenfunctions. This operation is also referred to as the Koopman mode decomposition, and $\mathbf{v}_j$ are the Koopman modes [20]:

$$\mathbf{v}_j = \begin{bmatrix} \langle\phi_i, g_1\rangle \\ \langle\phi_i, g_2\rangle \\ \vdots \\ \langle\phi_i, g_m\rangle \end{bmatrix} \tag{6}$$

The partial differential equation (4) is approximated using the Galerkin method to determine the eigenfunctions [26], and eventually a linear representation of the system. The idea is to project the Koopman operator onto a subspace that is defined by orthonormal basis functions. These projections $\langle\cdot\rangle$ are computed using the inner product of two functions $f_1(\mathbf{x})$ and $f_2(\mathbf{x})$:

$$\langle f_1(\mathbf{x}), f_2(\mathbf{x})\rangle = \int_{\Omega} f_1(\mathbf{x}) f_2(\mathbf{x}) w(\mathbf{x})\mathrm{d}\mathbf{x} \tag{7}$$

where $w(\mathbf{x})$ is a weighting function. In this work, we use orthonormal Legendre polynomials in the domain $\Omega = [-1, 1]$ and $w(\mathbf{x}) = 1$. Defining L_j as the jth basis function and recalling Eq. (2), we can write

$$\frac{\mathrm{d}L_i(\mathbf{x})}{\mathrm{d}t} = \frac{\mathrm{d}L_i(\mathbf{x})}{\mathrm{d}t} = (\nabla_{\mathbf{x}} L_i(\mathbf{x}))\mathbf{f}(\mathbf{x}) \tag{8}$$

Using the inner product, the Koopman operator (and thus, the derivatives) can be projected onto the basis functions to obtain a finite-dimensional matrix representation of $\mathcal{K}$ [26]:

$$K_{ij} = \langle(\nabla_{\mathbf{x}} L_i(\mathbf{x}))\mathbf{f}(\mathbf{x}), L_j(\mathbf{x})\rangle = \int_{\Omega} (\nabla_{\mathbf{x}} L_i(\mathbf{x}))\mathbf{f}(\mathbf{x}) L_j(\mathbf{x}) w(\mathbf{x})\mathrm{d}\mathbf{x} \tag{9}$$

where K_{ij} defines the elements of the Koopman matrix $\mathbf{K}$. Considering all basis functions, Eq. (2) can be rewritten as

$$\frac{\mathrm{d}}{\mathrm{d}t}\mathbf{L}(\mathbf{x}) = \mathbf{K}\mathbf{L} \tag{10}$$

where $\mathbf{L} = [L_1, L_2, \ldots, L_m]$ is a vector of m basis functions. This representation allows us to perform the eigendecomposition of $\mathbf{K}$ if $\mathbf{K}$ is diagonalizable. Defining $\mathbf{\Phi}(\mathbf{x}(\mathbf{t})) \coloneqq \mathbf{V}_r^{-1}\mathbf{L}(\mathbf{x}(t))$ as the vector of eigenfunctions with $\mathbf{V}_r$ being the matrix that contains the right eigenvectors in its columns, the evolution of the observable functions can be computed using

$$\begin{aligned}\mathbf{g}(\mathbf{x}(t)) &= \mathbf{P}\mathbf{L}(\mathbf{x}(t)) = \mathbf{P}\mathbf{V}_r\mathbf{\Phi}(\mathbf{x}(t)) = \mathbf{P}\mathbf{V}_r\mathrm{e}^{\mathbf{D}t}\mathbf{\Phi}(\mathbf{x}(t_0)) \\ &= \mathbf{P}\mathbf{V}_r\mathrm{e}^{\mathbf{D}t}\mathbf{V}_r^{-1}\mathbf{L}(\mathbf{x}(t_0))\end{aligned} \tag{11}$$

where $\mathbf{P}$ denotes the projections of $\mathbf{x}$ onto the basis functions, and $\mathbf{D}$ is a diagonal matrix of eigenvalues. Note that we are interested in the identity observable in this work, and hence $\mathbf{g}(\mathbf{x}) \equiv \mathbf{x}$.

Bilinearization of Control-Affine System. Adding an external control $\mathbf{u}$, the new dynamical system reads

$$\dot{\mathbf{x}} = \mathbf{f}(\mathbf{x}, \mathbf{u}) \tag{12}$$

We redefine the states and controls such that we can rewrite the original system in a control-affine form

$$\begin{aligned}\dot{\mathbf{x}} &= \mathbf{p}(\mathbf{x}) + \mathbf{B}(\mathbf{x})\mathbf{u} \\ &= \mathbf{p}(\mathbf{x}) + \sum_{i=1}^{q} \mathbf{b}_i u_i\end{aligned} \tag{13}$$

with $\mathbf{x}$ and $\mathbf{u}$ being the states and controls, respectively, and $\mathbf{b}_i(\mathbf{x})$ being the q columns of $\mathbf{B}(\mathbf{x})$. Let $\mathbf{T}(\mathbf{x}) = [T_1(\mathbf{x}), \ldots, T_l(\mathbf{x})]^\top$ be a vector of l eigenfunctions related to the dynamics $\mathbf{p}(\mathbf{x})$ (i.e. the unactuated system) whose ith entry is defined as follows [29]:

$$T_i(\mathbf{x}) = \phi_i(\mathbf{x}) \quad \text{if } \phi_i(\mathbf{x}) \in \mathbb{R} \tag{14}$$

$$[T_i(\mathbf{x}), T_{i+1}(\mathbf{x})]^\top = [2\,\mathrm{Re}(\phi_i(\mathbf{x})), -2\,\mathrm{Im}(\phi_{i+1}(\mathbf{x}))]^\top \quad \text{if } \phi_i(\mathbf{x}) \in \mathbb{C} \tag{15}$$

where ϕ_{i+1} is the complex conjugate of ϕ_i. The Koopman matrices $\mathbf{K}^{b_i}$ with respect to the control vector fields $\mathbf{b}_i$ can be obtained by calculating $\mathcal{K}^{b_i}(\mathbf{T}(\mathbf{x}))$:

$$K_{jk}^{b_i} = \left\langle \frac{\mathrm{d}T_j^{b_i}}{\mathrm{d}t}, L_k \right\rangle \tag{16}$$

The total derivatives are given by:

$$\frac{\mathrm{d}T_j}{\mathrm{d}t} = \frac{\partial T_j}{\partial x_1} b_{i,1} + \frac{\partial T_j}{\partial x_2} b_{i,2} + \cdots = \sum_{k=1}^{n} \frac{\partial T_j}{\partial x_k} b_{i,k} \tag{17}$$

where n is the number of states. Assuming that the Koopman operators with respect to the control vector fields lie in the span of the eigenfunctions corresponding to the unactuated system, Eq. (13) can be transformed into a bilinear system [29]:

$$\dot{\mathbf{z}} = \mathbf{D}\mathbf{z} + \sum_{i=1}^{q} \mathbf{E}_i \mathbf{z} u_i \tag{18a}$$

$$\mathbf{x} = \mathbf{C}\mathbf{z} \tag{18b}$$

with the transformed states $\mathbf{z}$, and constant matrices $\mathbf{D}$, $\mathbf{E}$, and $\mathbf{C}$. $\mathbf{D}$ is a block diagonal matrix with the entry $D_{i,i} = \lambda_i$ (λ_i being the eigenvalue associated with the eigenfunction ϕ_i) if ϕ_i is real-valued. Otherwise,

$$\begin{bmatrix} D_{i,i} & D_{i,i+1} \\ D_{i+1,i} & D_{i+1,i+1} \end{bmatrix} = |\lambda_i| \begin{bmatrix} \cos\left(\mathrm{Arg}\left(\lambda_i\right)\right) & \sin\left(\mathrm{Arg}\left(\lambda_i\right)\right) \\ -\sin\left(\mathrm{Arg}\left(\lambda_i\right)\right) & \cos\left(\mathrm{Arg}\left(\lambda_i\right)\right) \end{bmatrix} \tag{19}$$

where $\mathrm{Arg}\left(\cdot\right)$ denotes the argument of a complex number. $\mathbf{E}_i$ are comprised of the Koopman modes of $\mathcal{K}^{b_i}(\mathbf{T}(\mathbf{x}))$, and $\mathbf{C}$ contains the Koopman modes of the observable. This system describes the evolution of the eigenfunctions $\mathbf{z} \equiv \mathbf{T}(\mathbf{x})$ instead of the original states $\mathbf{x}$. These can be retrieved using the linear relationship in Eq. (18b).

OPTIMAL CONTROL PROBLEM

Even though the projection of the Koopman operator onto a finite subspace allows us to calculate the eigenfunctions and thus, the evolution of the states, it is important to understand that this is only an approximation. We can only use a limited number of basis functions and eigenfunctions, and therefore, the approximation is more accurate the more linear the original system is. With regard to the low-thrust trajectory optimization problem, we make use of a set of orbital elements that results in a linear representation for the unperturbed case. As the control actions are small due to the low-thrust propulsion, the problem can be considered a perturbation problem where the control term is small compared to the linear, unperturbed term. This section addresses the set of coordinates and extends the equations of motion to the case when controls are present. Moreover, the optimal control problem is stated.

Set of Orbital Elements

Defining the six orbital elements as $[\Lambda, \eta, s, \gamma, \kappa, \beta]$, the equations of motions read in the unperturbed case [26]

$$\frac{\mathrm{d}\Lambda}{\mathrm{d}\tau} = -\eta \tag{20a}$$
$$\frac{\mathrm{d}\eta}{\mathrm{d}\tau} = \Lambda \tag{20b}$$
$$\frac{\mathrm{d}s}{\mathrm{d}\tau} = \gamma \tag{20c}$$
$$\frac{\mathrm{d}\gamma}{\mathrm{d}\tau} = -s \tag{20d}$$
$$\frac{\mathrm{d}\kappa}{\mathrm{d}\tau} = 0 \tag{20e}$$
$$\frac{\mathrm{d}\beta}{\mathrm{d}\tau} = 0 \tag{20f}$$

Their relationship to spherical coordinates is given by

$$\Lambda = \frac{p_\theta}{r} - \frac{\mu}{p_\theta}\sqrt{\frac{\mathrm{LU}}{\mu}} \tag{21}$$

$$\eta = p_r\sqrt{\frac{\mathrm{LU}}{\mu}} \tag{22}$$

$$s = \sin(\phi) \tag{23}$$

$$\gamma = \frac{p_\varphi}{p_\theta}\cos(\varphi) \tag{24}$$

$$\kappa = \frac{1}{p_\theta}\sqrt{\mu\,\mathrm{LU}} \tag{25}$$

where p_r, p_λ, and p_φ are the conjugate momenta of the corresponding Hamiltonian,

$$p_r = \dot{r} \tag{26}$$

$$p_\lambda = r^2\dot{\lambda}\cos^2(\varphi) \tag{27}$$

$$p_\varphi = r^2\dot{\varphi} \tag{28}$$

and p_θ is the angular momentum:

$$p_\theta = \sqrt{p_\phi^2 + \frac{p_\lambda^2}{\cos^2(\phi)}} \tag{29}$$

r denotes the radial distance, λ and φ the azimuthal and polar angle, respectively. The standard gravitational parameter μ and some length unit LU are included to make the quantities dimensionless. This is important as we use Legendre polynomials for the basis functions that are defined in the domain $[-1, 1]$. Therefore, it is to be ensured that the values of the coordinates stay within this range. Otherwise, their behavior cannot be captured accurately, and accuracy and convergence can deteriorate. β is identical to the classical longitude of the ascending node. Note that a Sundman transformation was performed, and Eqs. (20a)–(20f) are written in the τ domain that is defined as follows:

$$\frac{\mathrm{d}\tau}{\mathrm{d}t} = \frac{p_\theta}{r^2} \tag{30}$$

The time can thus be obtained by integrating the following differential equation:

$$\frac{\mathrm{d}t}{\mathrm{d}\tau} = \frac{1}{\kappa(\kappa+\Lambda)^2}\sqrt{\frac{\mathrm{LU}^3}{\mu}} \tag{31}$$

The equations of motion with a perturbing acceleration $\mathbf{a}_p$ can be determined by computing the partial derivatives of each orbital element $\mathcal{O}$ with respect to the velocity $\mathbf{v}$ [30]:

$$\frac{\mathrm{d}\mathcal{O}}{\mathrm{d}t} = \frac{\mathrm{d}\mathcal{O}}{\mathrm{d}t}\Big|_{\text{unpert.}} + \frac{\partial\mathcal{O}}{\partial\mathbf{v}}\mathbf{a}_p, \qquad \mathcal{O} \in \{\Lambda, \eta, s, \gamma, \kappa, \beta\} \tag{32}$$

where the first term on the right-hand side refers to the unperturbed dynamics in Eqs. (20a)–(20f), and the second term to the perturbation. We write the acceleration vector in the standard local-vertical local-horizontal rotating frame:

$$\mathbf{a}_p = a_r\,\mathbf{i}_r + a_t\,\mathbf{i}_t + a_n\,\mathbf{i}_n \tag{33}$$

where the first axis is the radial unit vector $\mathbf{i}_r = \mathbf{r}/r$ that points along the position vector. The normal unit vector $\mathbf{i}_n$ points in the orbit normal direction with $\mathbf{r} \times \mathbf{v} = p_\theta \, \mathbf{i}_n$. The transversal unit vector $\mathbf{i}_t$ is found with the right-hand rule. Using the definition of the elements, the chain rule, and the fact that the state components are independent, the equations of motion are found to be:

$$\frac{\mathrm{d}\Lambda}{\mathrm{d}\tau} = -\eta + \frac{2\kappa + \Lambda}{\kappa(\kappa+\Lambda)^3} \frac{\mathrm{LU}^2}{\mu} a_t \tag{34a}$$

$$\frac{\mathrm{d}\eta}{\mathrm{d}\tau} = \Lambda + \frac{1}{\kappa(\kappa+\Lambda)^2} \frac{\mathrm{LU}^2}{\mu} a_r \tag{34b}$$

$$\frac{\mathrm{d}s}{\mathrm{d}\tau} = \gamma \tag{34c}$$

$$\frac{\mathrm{d}\gamma}{\mathrm{d}\tau} = -s + \frac{\sqrt{1-s^2-\gamma^2}}{\kappa(\kappa+\Lambda)^3} \frac{\mathrm{LU}^2}{\mu} a_n \tag{34d}$$

$$\frac{\mathrm{d}\kappa}{\mathrm{d}\tau} = -\frac{1}{(\kappa+\Lambda)^3} \frac{\mathrm{LU}^2}{\mu} a_t \tag{34e}$$

$$\frac{\mathrm{d}\beta}{\mathrm{d}\tau} = \frac{s}{(s^2+\gamma^2)\kappa(\kappa+\Lambda)^3} \frac{\mathrm{LU}^2}{\mu} a_n \tag{34f}$$

$$\tag{34g}$$

Low-Thrust Trajectory Optimization Problem

The general optimal control problem can be written as

$$\underset{\mathbf{u}(t)}{\text{minimize}} \quad J(\mathbf{x}(t), \mathbf{u}(t)) \tag{35a}$$

$$\text{subject to:} \quad \dot{\mathbf{x}}(t) = \mathbf{f}(\mathbf{x}(t), \mathbf{u}(t)) \tag{35b}$$

$$\mathbf{h}(\mathbf{x}(t), \mathbf{u}(t)) \leq \mathbf{0} \tag{35c}$$

$$\mathbf{\Psi}(\mathbf{x}(t_0), \mathbf{x}(t_f)) = \mathbf{0} \tag{35d}$$

where $J(\mathbf{x}(t), \mathbf{u}(t))$ is the performance index and Eqs. (35b)–(35d) are the dynamical, path, and endpoint constraints, respectively. In this work, we intend to solve the low-thrust energy-optimal problem. For demonstration purposes, we consider a planar, fixed final time rendezvous problem. Note, however, that it is straightforward to extend the approach to three-dimensional transfers. Therefore, only the elements Λ, η, and κ are considered as they are affected by the perturbing accelerations a_t and a_s in the orbital plane. The states and controls are defined as $\mathbf{x} = [\Lambda, \eta, \kappa, t]^\top$ and $\mathbf{u} = [a_t, a_r, a]^\top$, respectively, where the time t is included to target a specific time, and $a = \left\| [a_t, a_r]^\top \right\|_2$ is the magnitude of the acceleration. For simplicity, the time rate of change of the mass is neglected. The dynamics then read

$$\mathbf{f}(\mathbf{x}, \mathbf{u}) = \begin{bmatrix} \eta' \\ \Lambda' \\ \kappa' \\ t' \end{bmatrix} = \begin{bmatrix} -\eta \\ \Lambda \\ 0 \\ \frac{1}{\kappa(\kappa+\Lambda)^2} \sqrt{\mathrm{LU}^3/\mu} \end{bmatrix} + \begin{bmatrix} 0 \\ \frac{1}{\kappa(\kappa+\Lambda)^2} \mathrm{LU}^2/\mu \\ 0 \\ 0 \end{bmatrix} a_r + \begin{bmatrix} \frac{2\kappa+\Lambda}{\kappa(\kappa+\Lambda)^3} \mathrm{LU}^2/\mu \\ 0 \\ -\frac{1}{(\kappa+\Lambda)^3} \mathrm{LU}^2/\mu \\ 0 \end{bmatrix} a_t \tag{36}$$

where $(\cdot)'$ denotes the derivative with respect to τ. After transforming the coordinates into the extended configuration space $\mathbf{z} = \mathbf{T}(\mathbf{x})$ and calculating the matrices $\mathbf{D}$, $\mathbf{E}_1$, $\mathbf{E}_2$, and $\mathbf{C}$ according

to the previous section, the optimal control problem is given by

$$\underset{\mathbf{u}}{\text{minimize}} \quad \int_{\tau_0}^{\tau_f} a^2 \, \mathrm{d}\tau \tag{37a}$$

$$\text{subject to:} \quad \mathbf{z}' = \begin{bmatrix} \mathbf{z}_1' \\ z_2' \end{bmatrix} = \begin{bmatrix} \mathbf{D}\mathbf{z} + \mathbf{E}_1\mathbf{z}a_r + \mathbf{E}_2\mathbf{z}a_t \\ \frac{1}{\kappa(\kappa+\Lambda)^2}\sqrt{\mathrm{LU}^3/\mu} \end{bmatrix} \tag{37b}$$

$$\left\| \begin{bmatrix} a_r \\ a_t \end{bmatrix} \right\|_2 = a \tag{37c}$$

$$\mathbf{z}(\tau_0) = \mathbf{z}_0, \quad \mathbf{z}(\tau_f) = \mathbf{z}_f \tag{37d}$$

$$\mathbf{z}_l \leq \mathbf{z} \leq \mathbf{z}_u, \quad \mathbf{u}_l \leq \mathbf{u} \leq \mathbf{u}_u \tag{37e}$$

$\mathbf{z}_1$ and z_2 refer to the entries of $\mathbf{z}$ that correspond to the orbital elements and time, respectively. $\mathbf{z}_0$ is the initial state at τ_0, and $\mathbf{z}_f$ is the desired final state at τ_f. The subscripts l and u denote the lower and upper bounds of states and controls, respectively.

NUMERICAL SIMULATIONS

We consider an interplanetary transfer from the Sun-Earth Lagrange point L_2 (SEL_2) to near-Earth asteroid 2000 SG344. This is one of the potential targets of ESA's Miniaturised Asteroid Remote Geophysical Observer (M-ARGO) mission [10]. The nonlinear program is solved with the optimal control software GPOPS-II [31] and the Interior Point Optimizer IPOPT [32]. Physical constants of the simulation are given in Table 1, and the parameters for the transfer in Table 2. We briefly assess the accuracy of the transformed dynamical system before addressing the transfer.

Table 1: Physical constants in all simulations.

Parameter	Value
Gravitational constant μ	$1.32712 \times 10^{11}\ \mathrm{km}^3/\mathrm{s}^2$
Gravitational acceleration g_0	$9.80665 \times 10^{-3}\ \mathrm{km}/\mathrm{s}^2$
Length unit LU	$0.9 \cdot 1.49597 \times 10^8$ km
Velocity unit VU	$\sqrt{\mu/\mathrm{LU}}$ km/s
Time unit TU	LU/VU s
Acceleration unit ACU	VU/TU km/s^2
Mass unit MU	$m(t_0)$

Table 2: Parameters for SEL_2 to asteroid 2000 SG344 transfer.

Parameter	Value
Initial epoch	04-Feb-2024 12:00:00 UTC
Time of flight t_f	700 days
Initial mass $m(t_0)$	22.6 kg
Maximum acceleration a_{max}	$10^{-7}\ \mathrm{km}/\mathrm{s}^2$

Accuracy of the Bilinear System

As only a finite number of eigenfunctions and basis functions is used, the obtained bilinear system is only an approximation of the real nonlinear dynamics. In order to assess the accuracy of the approximation, we propagate the transformed dynamics in Eq. (37b) and the real dynamics in Eq. (34) and compare the results. The dynamics are integrated for a period of 890 days (approximately two revolutions) with the following thrust profile:

$$\mathbf{a} = \begin{cases} \mathbf{a}_{\text{max}}, & \text{if } t \in [0, 100] \text{ days} \\ \mathbf{a}_{\text{max}}, & \text{if } t \in [400, 500] \text{ days} \\ \mathbf{a}_{\text{max}}, & \text{if } t \in [700, 800] \text{ days} \\ \mathbf{0}, & \text{otherwise} \end{cases} \tag{38}$$

where $\mathbf{a}_{\text{max}} = a_{\text{max}} \cdot [0.7, 0.7141]^\top = 10^{-7}\ \text{km/s}^2 \cdot [0.7, 0.7141]^\top$. The distribution and length of the thrust arcs is based on typical thrust profiles of the M-ARGO mission [10]. Figure 1 shows the position error for basis functions of orders 3 to 7. It is evident that using third order polynomials results in a large error of 10^5 km throughout the transfer (see Fig. 1a). As expected, these polynomials cannot represent the dynamical system accurately as fourth order terms appear in the denominator of Λ' in Eq. (34a). Therefore, Fig. (1b) illustrates the behavior of the orders 4 to 7 only. Remarkably, the errors decrease by one order of magnitude to a maximum value of 10^4 km. Regardless of the polynomial degree, the error is small at the beginning and increases over time. Still, the error can be reduced significantly if higher orders are used. As we consider an interplanetary transfer where the length scales are in the order of an astronomical unit, an error of 10^3 to 10^4 km is often considered acceptable for the cruise phase. Moreover, if a direct method is used to solve the optimal control problem, the trajectory is divided into segments, and the dynamics need to be accurate only for a short time period. Therefore, even lower orders can yield accurate results for the transfer considered in this work. Note that the behavior of the velocity error is similar as can be observed in Figs. 1c and 1d.

Low-Thrust Trajectory Optimization

The feasibility and optimality tolerances of IPOPT are set to 10^{-6} and 10^{-5}, respectively. We use 40 segments with 5 nodes each. Basis functions of orders 3 to 7 are chosen. Regardless of the order, the solver was able to find optimal solutions that are identical to the one obtained with the real nonlinear dynamics. Figure 2a illustrates the optimized trajectory, and the acceleration magnitude is shown in Fig. 2b. Clearly, the characteristic smooth behavior of energy-optimal profiles can be observed, i.e. neither bang-bang (fuel-optimal) nor full thrust at all times (time-optimal). The evolution of all orbital elements is given in Fig. 3, including the ones that are not affected by perturbations in the orbital plane. Λ, η, s, and γ show the characteristic periodic behavior, whereas κ behaves like the inverse of the specific angular momentum; β, instead, is constant. Similar to the previous subsection, we compare the accuracy for different orders of the basis functions in Fig. 4. This time, the dynamics of the bilinear and real system are integrated using the obtained controls. As expected, the propagation error decreases for higher orders. Still, the overall error is significantly smaller compared to propagating in one shot. Remarkably, even the third order can achieve an acceptable accuracy when a direct collocation approach is used. Interestingly, the number of iterations required by the solver is up to $50\,\%$ lower for the bilinear system compared to the original one. Yet, the CPU time can increase considerably from few seconds (low orders) to minutes (high orders).

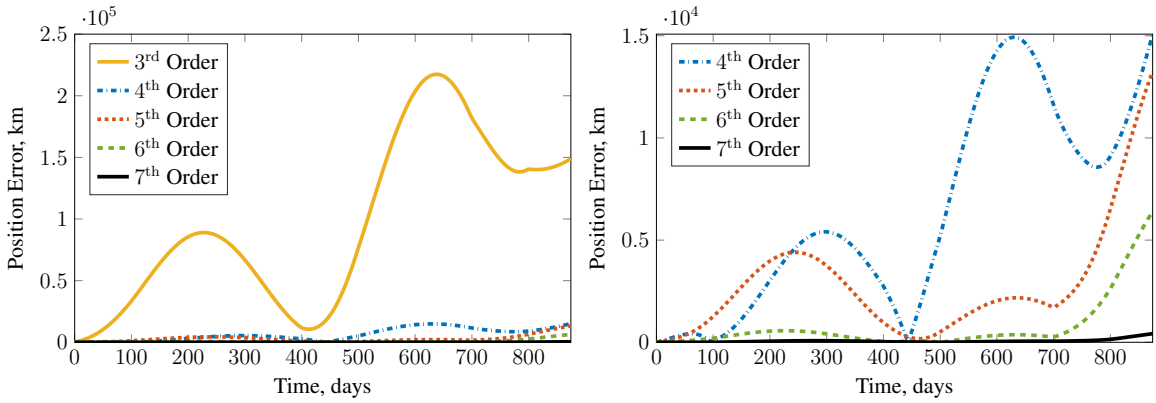

(a) Position error for basis function orders 3 to 7.

(b) Position error for basis function orders 4 to 7.

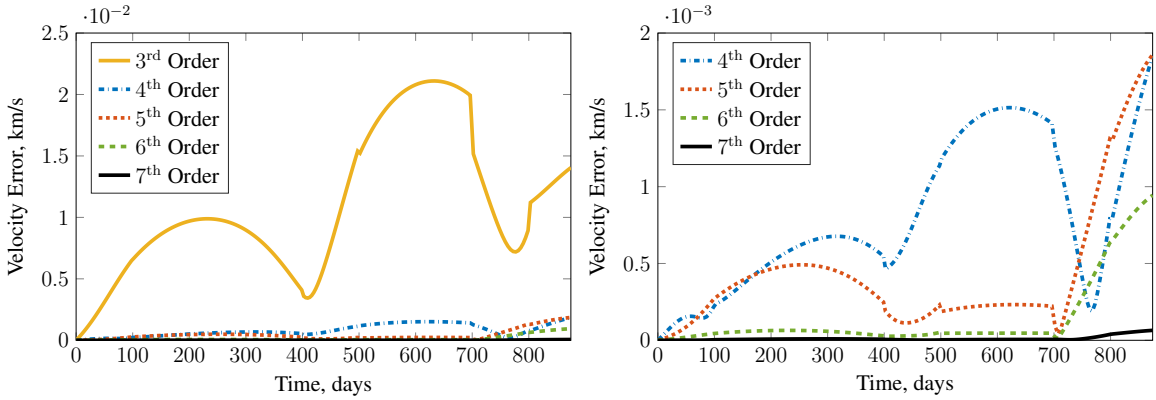

(c) Velocity error for basis function orders 3 to 7.

(d) Velocity error for basis function orders 4 to 7.

Figure 1: Position and velocity errors for basis function orders 3 to 7.

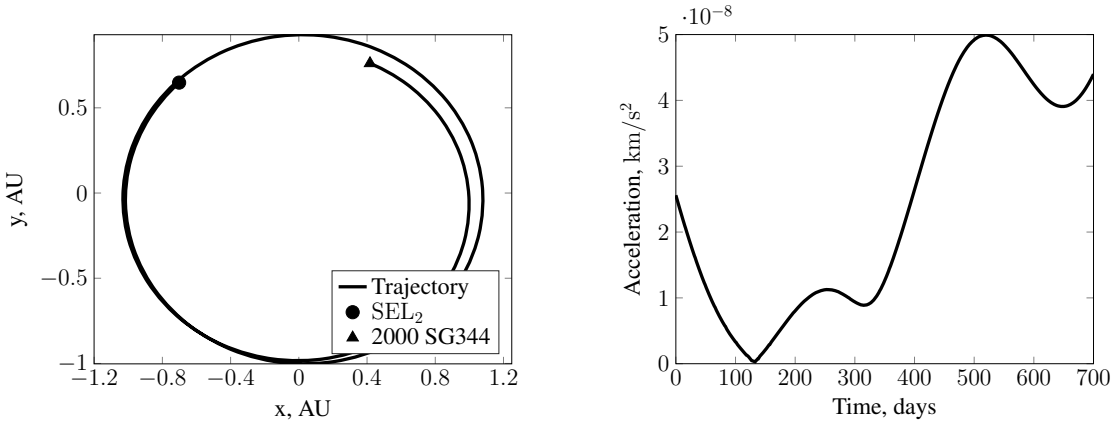

(a) Trajectory

(b) Acceleration profile

Figure 2: Transfer trajectory from SEL_2 to asteroid 2000 SG344 and the corresponding acceleration profile.

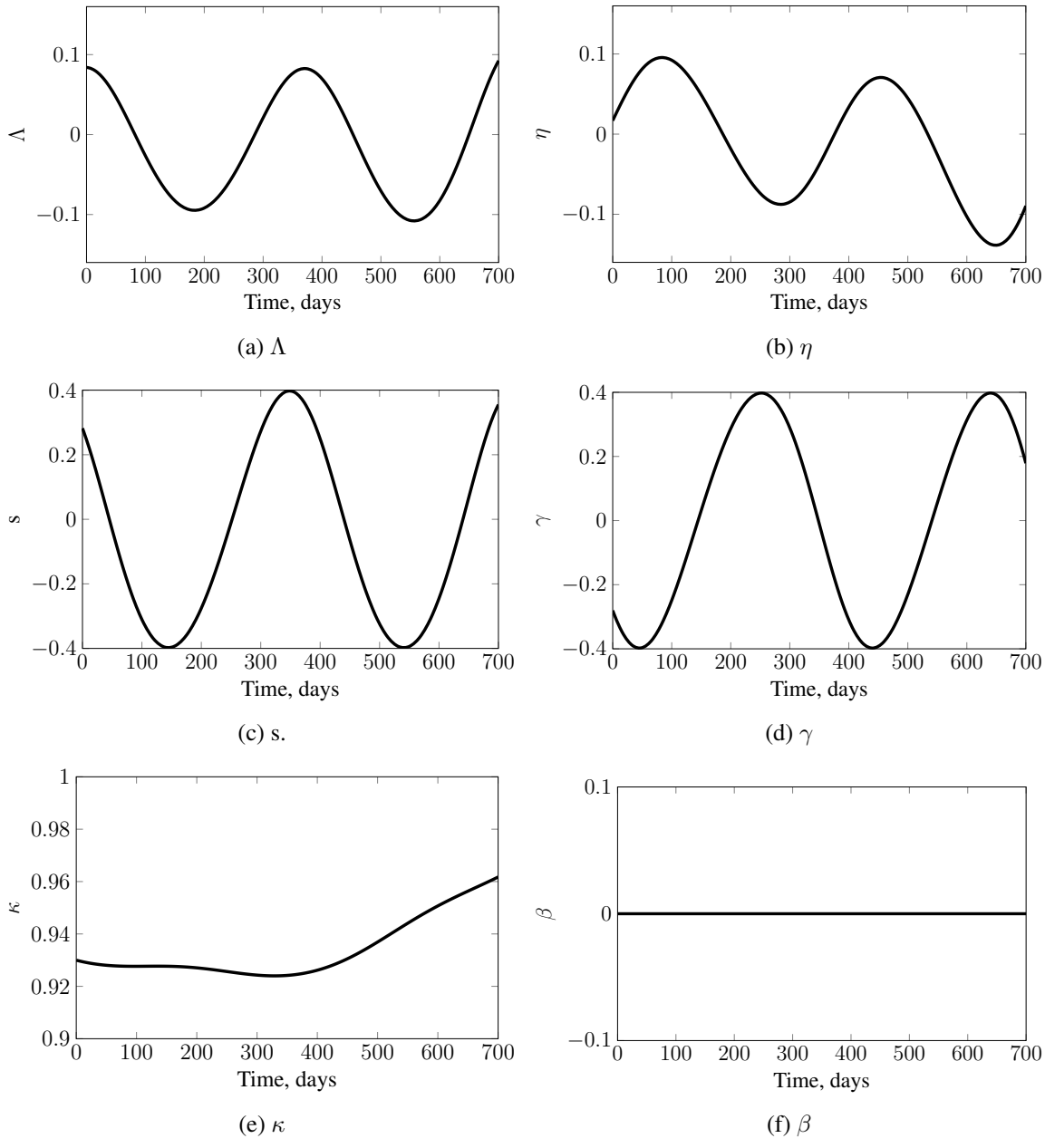

(a) Λ (b) η

(c) s. (d) γ

(e) κ (f) β

Figure 3: Evolution of the orbital elements.

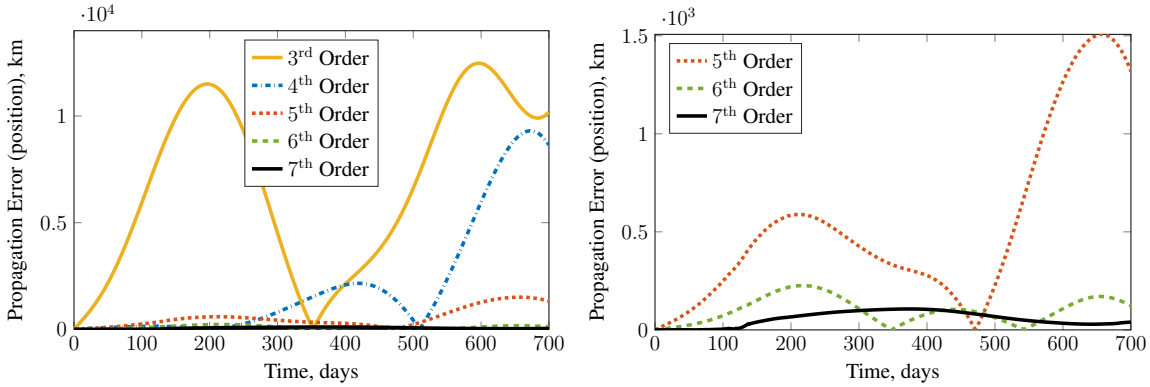

(a) Propagation error for basis function orders 3 to 7. (b) Propagation error for basis function orders 5 to 7.

Figure 4: Propagation error (position) for basis function orders 3 to 7.

CONCLUSION

This work presents the Koopman operator theory to reduce the complexity of nonlinear optimal control problems. It was shown that the dynamics of the low-thrust trajectory optimization problem can be transformed into a bilinear system using a new set of orbital elements. Even though this approach requires some effort to transform the dynamical system into a higher-dimensional space, this needs to be done only once. Preliminary results show that such a global approximation can yield a sufficient level of accuracy even for lower-order basis functions. The Koopman operator theory is therefore an interesting approach to address nonlinear systems, also within an optimal control framework. Still, one of the open challenges is to handle the higher-dimensional space properly.

REFERENCES

[1] M. D. Rayman, P. A. Chadbourne, J. S. Culwell, and S. N. Williams, "Mission design for deep space 1: A low-thrust technology validation mission," *Acta Astronautica*, Vol. 45, No. 4, 1999, pp. 381–388, 10.1016/S0094-5765(99)00157-5.

[2] E. Adams, D. O'Shaughnessy, M. Reinhart, J. John, E. Congdon, D. Gallagher, E. Abel, J. Atchison, Z. Fletcher, M. Chen, C. Heistand, P. Huang, E. Smith, D. Sibol, D. Bekker, and D. Carrelli, "Double Asteroid Redirection Test: The Earth Strikes Back," *2019 IEEE Aerospace Conference*, 2019, pp. 1–11, 10.1109/AERO.2019.8742007.

[3] D. M. Di Cara and D. Estublier, "Smart-1: An analysis of flight data," *Acta Astronautica*, Vol. 57, No. 2, 2005, pp. 250–256, 10.1016/j.actaastro.2005.03.036.

[4] A. Poghosyan and A. Golkar, "CubeSat Evolution: Analyzing CubeSat Capabilities for Conducting Science Missions," *Progress in Aerospace Sciences*, Vol. 88, 2017, pp. 59–83, doi: 10.1016/j.paerosci.2016.11.002.

[5] A. Slavinskis and e. al., "Nanospacecraft fleet for multi-asteroid touring with electric solar wind sails," *2018 IEEE Aerospace Conference*, 2018, pp. 1–20, 10.1109/AERO.2018.8396670.

[6] A. Klesh and J. Krajewski, "MarCO: Mars Cube One – Lessons Learned from Readying the First Interplanetary Cubesats for Flight," *49th Lunar and Planetary Science Conference*, 2018.

[7] M. B. Quadrelli and e. al., "Guidance, Navigation, and Control Technology Assessment for Future Planetary Science Missions," *Journal of Guidance, Control, and Dynamics*, Vol. 38, No. 7, 2015, pp. 1165–1186, 10.2514/1.G000525.

[8] P. Tsiotras and M. Mesbahi, "Toward an Algorithmic Control Theory," *Journal of Guidance, Control, and Dynamics*, Vol. 40, No. 2, 2017, pp. 194–196, 10.2514/1.G002754.

[9] L. Blackmore, "Autonomous Precision Landing of Space Rockets," *The Bridge*, Vol. 4, No. 46, 2016, pp. 15–20.

[10] F. Topputo, Y. Wang, G. Giordano, V. Franzese, H. Goldberg, F. Perez-Lissi, and R. Walker, "Envelop of Reachable Asteroids by M-ARGO CubeSat," *Advances in Space Research*, Vol. 67, No. 12, 2021, pp. 4193–4221, 10.1016/j.asr.2021.02.031.

[11] J. T. Betts, "Survey of Numerical Methods for Trajectory Optimization," *Journal of Guidance, Control, and Dynamics*, Vol. 21, No. 2, 1998, pp. 193 – 207, 10.2514/2.4231.

[12] G. Lantoine and R. P. Russell, "The Stark Model: an exact, closed-form approach to low-thrust trajectory optimization," *21st International Symposium on Space Flight Dynamics*, 2009.

[13] E. Taheri and O. Abdelkhalik, "Initial Three-Dimensional Low-Thrust Trajectory Design," *Advances in Space Research*, Vol. 57, No. 3, 2016, pp. 889 – 903, 10.1016/j.asr.2015.11.034.

[14] C. Bombardelli, G. Baù, and J. Peláez, "Asymptotic solution for the two-body problem with constant tangential thrust acceleration," *Celestial Mechanics and Dynamical Astronomy*, Vol. 110, No. 3, 2011, p. 239–256, 10.1016/j.asr.2021.02.031.

[15] Y. Mao, M. Szmuk, and B. Açıkmeşe, "A Tutorial on Real-time Convex Optimization Based Guidance and Control for Aerospace Applications," *2018 Annual American Control Conference (ACC)*, 2018, pp. 2410–2416, 10.23919/ACC.2018.8430984.

[16] C. Hofmann and F. Topputo, "Rapid Low-Thrust Trajectory Optimization in Deep Space Based On Convex Programming," *Journal of Guidance, Control, and Dynamics*, Vol. 44, No. 7, 2021, pp. 1379–1388, 10.2514/1.G005839.

[17] D. Malyuta, Y. Yu, P. Elango, and B. Açıkmeşe, "Advances in trajectory optimization for space vehicle control," *Annual Reviews in Control*, Vol. 52, 2021, pp. 282–315, 10.1016/j.arcontrol.2021.04.013.

[18] X. Liu, P. Lu, and B. Pan, "Survey of Convex Optimization for Aerospace Applications," *Astrodynamics*, Vol. 1, No. 1, 2017, pp. 23–40, 10.1007/s42064-017-0003-8.

[19] H. Harry Asada and F. E. Sotiropoulos, "Dual Faceted Linearization of Nonlinear Dynamical Systems Based on Physical Modeling Theory," *Journal of Dynamic Systems, Measurement, and Control*, Vol. 141, 10 2018, 10.1115/1.4041448.

[20] S. L. Brunton, M. Budišić, E. Kaiser, and J. N. Kutz, "Modern Koopman Theory for Dynamical Systems," `https://arxiv.org/abs/1804.06539`, Preprint.

[21] M. Budišić, R. Mohr, and I. Mezić, "Applied Koopmanism," *Chaos: An Interdisciplinary Journal of Nonlinear Science*, Vol. 22, No. 4, 2012, p. 047510, 10.1063/1.4772195.

[22] S. E. Otto and C. W. Rowley, "Koopman Operators for Estimation and Control of Dynamical Systems," *Annual Review of Control, Robotics, and Autonomous Systems*, Vol. 4, No. 1, 2021, pp. 59–87, 10.1146/annurev-control-071020-010108.

[23] M. L. Castaño, A. Hess, G. Mamakoukas, T. Gao, T. Murphey, and X. Tan, "Control-oriented Modeling of Soft Robotic Swimmer with Koopman Operators," *2020 IEEE/ASME International Conference on Advanced Intelligent Mechatronics (AIM)*, 2020, pp. 1679–1685, 10.1109/AIM43001.2020.9159033.

[24] I. Mezić, "Analysis of Fluid Flows via Spectral Properties of the Koopman Operator," *Annual Review of Fluid Mechanics*, Vol. 45, No. 1, 2013, pp. 357–378, 10.1146/annurev-fluid-011212-140652.

[25] S. Servadio, D. Arnas, and R. Linares, "Dynamics Near the Three-Body Libration Points via Koopman Operator Theory," *Journal of Guidance, Control, and Dynamics*, Vol. 0, No. 0, 0, pp. 1–15, 10.2514/1.G006519.

[26] D. Arnas and R. Linares, "Approximate Analytical Solution to the Zonal Harmonics Problem Using Koopman Operator Theory," *Journal of Guidance, Control, and Dynamics*, Vol. 44, No. 11, 2021, pp. 1909–1923, 10.2514/1.G005864.

[27] T. Chen and J. Shan, "Koopman-Operator-Based Attitude Dynamics and Control on SO(3)," *Journal of Guidance, Control, and Dynamics*, Vol. 43, No. 11, 2020, pp. 2112–2126, 10.2514/1.G005006.

[28] R. Linares, "Koopman Operator Theory Applied to the Motion of Satellites," *AAS/AIAA Astrodynamics Specialist Conference*, August Aug. 2019. AAS Paper 19-821.

[29] D. Goswami and D. A. Paley, "Global bilinearization and controllability of control-affine nonlinear systems: A Koopman spectral approach," *2017 IEEE 56th Annual Conference on Decision and Control (CDC)*, 2017, pp. 6107–6112, 10.1109/CDC.2017.8264582.

[30] R. Battin, *An Introduction to the Mathematics and Methods of Astrodynamics*. AIAA Education Series, American Institute of Aeronautics & Astronautics, 1999.

[31] M. A. Patterson and A. V. Rao, "GPOPS-II: A MATLAB software for solving multiple-phase optimal control problems using hp-adaptive Gaussian quadrature collocation methods and sparse nonlinear programming," *ACM Transactions on Mathematical Software (TOMS)*, Vol. 41, No. 1, 2014, pp. 1–37.

[32] A. Wächter and L. T. Biegler, "Line Search Filter Methods for Nonlinear Programming: Motivation and Global Convergence," *SIAM Journal on Optimization*, Vol. 16, No. 1, 2005, pp. 1–31, 10.1137/S1052623403426556.